Journal Pre-proof

Consistency of Independent Component Analysis for FMRI

Wei Zhao (Conceptualization) (Software) (Data curation) (Writing - original draft), Huanjie Li (Conceptualization) (Methodology), Guoqiang Hu (Software), Yuxing Hao (Validation), Qing Zhang (Resources), Jianlin Wu (Resources), Blaise B. Frederick (Writing - review and editing) (Supervision), Fengyu Cong (Supervision) (Funding acquisition) (Project administration)

PII: S0165-0270(20)30436-2

DOI: https://doi.org/10.1016/j.jneumeth.2020.109013

Reference: NSM 109013

To appear in: *Journal of Neuroscience Methods*

Received Date: 26 July 2020

Revised Date: 23 November 2020

Accepted Date: 26 November 2020

Please cite this article as: Zhao W, Li H, Hu G, Hao Y, Zhang Q, Wu J, Frederick BB, Cong F, Consistency of Independent Component Analysis for FMRI, *Journal of Neuroscience Methods* (2020), doi: https://doi.org/10.1016/j.jneumeth.2020.109013

Consistency of Independent Component Analysis for FMRI

Wei Zhao[a,*], Huanjie Li [a,*], Guoqiang Hu[a], Yuxing Hao[a], Qing Zhang[b], Jianlin Wu[b], Blaise B.Frederick[c,**], Fengyu Cong[a,d,e,f,**]

[a] School of Biomedical Engineering, Faculty of Electronic Information and Electrical Engineering, Dalian University of Technology, Dalian, China

[b] Department of Radiology, Affiliated Zhongshan Hospital of Dalian University, Dalian, China

[c]Department of Psychiatry, Harvard Medical School, Harvard University, Boston, MA, USA

[d] School of Artificial Intelligence, Faculty of Electronic Information and Electrical Engineering, Dalian University of Technology, Dalian, China

[e] Key Laboratory of Integrated Circuit and Biomedical Electronic System, Liaoning Province. Dalian University of Technology, Dalian, China

[f] Faculty of Information Technology, University of Jyvaskyla, Jyvaskyla, Finland

Highlights

- ICA decomposition result of fMRI data changes when the model order varies.
- The consistency of components is distinguishing to tell signals and noises.
- Across model orders validation helps capture consistent components.
- Consistency can indicate the stability of the ICA decomposition results.

Abstract

Background: Independent component analysis (ICA) has been widely used for blind source separation in the field of medical imaging. However, despite of previous substantial efforts, the stability of ICA components remains a critical issue which has not been adequately addressed, despite numerous previous efforts. Most critical is the inconsistency of some of the extracted components when ICA is run with different model orders (MOs).

New Method: In this study, a novel method of determining the consistency of component analysis (CoCA) is proposed to evaluate the consistency of extracted components with different model orders. In the method, "consistent components" (CCs) are defined as those which can be extracted repeatably over a range of model orders.

Result: The efficacy of the method was evaluated with simulation data and fMRI datasets. With our method, the simulation result showed a clear difference of consistency between ground truths and noise.

Comparison with existing methods: The information criteria were implemented to provide suggestions for the optimal model order, where some of the ICs were revealed inconsistent in our proposed method.

Conclusions: This method provided an objective protocol for choosing CCs of an ICA

decomposition of a data matrix, independent of model order. This is especially useful with high model orders, where noise or other disturbances could possibly lead to an instability of the components.

Keywords: consistency; model order; ICA; fMRI.

1. Introduction

Independent component analysis (ICA), which separates the input signals into a complete set of maximally independent ones (Hyvärinen, 1999; J.Sejnowski, 1995), has been widely and increasingly applied in neuroimaging studies for the past two decades. ICA is an effective data-driven method, and is also preferred to model-driven methods like general linear model (GLM, Flandin and Friston, 2008) or dynamic causal modeling (DCM, Friston et al., 2003) when the research paradigm does not include any prior knowledge, or a second-level feature data (e.g. ALFF in fMRI, FA in DTI, which are features denoting physiology meaning without time course) is required in magnetic resonance imaging (MRI) studies. With the popularity of ICA in neuroimaging studies increases, there has been more scrutiny of the stability of extracted ICA components, due to the replicability crisis caused by the component instability (Artoni et al., 2014; Cong et al., 2014; Himberg et al., 2004; Levin-Schwartz et al., 2017).

The replicability of the ICA decomposition of a data matrix is a vital (but frequently ignored) problem that requires a solution, which has long been ignored. Factors, such as covariate effects, noise or disturbance, and differing experimental paradigms or neuro-imaging acquisition protocols, can alter the data subtly and cause instability of ICA decomposition results. Accumulative efforts have been devoted to address this issue by employing soft or aggressive denoising approaches (Griffanti et al., 2014; Pruim et al., 2015). In resting state human fMRI data, there has been an effort to define stable, reliable components, but in this case, reliability across subjects refers to homologous ICs (Celone et al., 2006; Damoiseaux et al., 2006) across subjects or reliability within-subjects (Cong et al., 2013; Groppe et al., 2009; Himberg et al., 2004) refers to the physiological plausibility and statistical reliability of each IC. Despite of the usefulness in the above context, this can only be a workaround, not a solution. Addressing the instability issue of ICA results, and allowing the selection of authentic and consistent ICs would greatly reduce the efforts for further physiological plausibility and statistical reliability analysis.

MELODIC ICA in FSL (Smith et al., 2004) and GIFT (Group ICA of fMRI Toolbox, Calhoun et al., 2010) are two of the most popular ICA software packages. However, the ease of use and great convenience provided by them means that they may lead to an inappropriate application in the hands of less experienced users who are not familiar with the limitation ICA regarding model order selection and reliability. In terms of a typical ICA procedure, the model order (the number of ICs to extract) is automatically determined using information criterion such as the well-known Akaike's

information criterion (AIC), Kullback Information Criterion (KIC), the minimum description length (MDL) criterion (Calhoun et al., 2010), or even straight-forward variance explanation percentage, especially when dimension reduction is performed using principal component analysis (PCA). However, the MO is likely to vary, even for one single dataset processed with different pre-processing protocols, especially when the dimensions of neuroimaging datasets are increasing. In addition, even with a small change of MO, for example 20 versus 25, some of the resulting ICs may differ significantly, for the reason that a larger amount of key information has been retained with the increased MO (Remes et al., 2011). Instead of repeatedly adjusting the MO when decomposed ICs cannot be properly interpreted by physiological plausibility and statistical reliability analysis, or simply accepting the ICA results in one single MO no matter how good or bad they are, this study attempts to propose a more comprehensive and rigorous method for objectively selecting the correct (and rejecting spurious) ICs.

The extracted components from ICA need to be evaluated before they can be used for further analyses. The ICA model usually includes one unmixing matrix and one source matrix, which in functional MRI studies also known as the time-course (this could be subject serial in second-level feature MRI data) and spatial distribution. Some studies (Meindl et al., 2010; Wisner et al., 2013) have proposed other alternative methods to evaluate the stability of ICA algorithms, mainly focusing on the spatial distribution (used for physiological plausibility); Some study (Hu et al., 2019) combined the spatial distribution and time-course (used for statistical reliability) as rank-1 spatial-temporal matrix accounting for a more convincing result. Both spatial and temporal aspects of the generated independent components could provide meaningful information. Therefore, assessment of spatiotemporal stability, via hierarchical cluster analysis of spatiotemporal tensors on a multi-dimensional rank-1 matrix, will provide more complete information regarding the balance between spatial and temporal stability, compared with either assessment separately. The tensor clustering results can be utilized to determine a reasonable MO range.

The CoCA method described above proposes that ICA can be implemented over a range of MOs and narrowed down to a reasonable range to achieve the goal of finding an optimal MO among this range, and then selecting the CCs within the group that is sufficiently consistent across all MOs. InfomaxICA (J.Sejnowski, 1995) and FastICA (Hyvärinen, 1999) are the two most frequently used ICA algorithms, and are therefore chosen for testing the stability performance. The ICA results are evaluated by using a correlation coefficient based index C_q (consistency quality, details provided in method section). CoCA excludes ICs which do not achieve a certain threshold level of C_q for further analyses.

2. Materials and methods

2.1. Simulation data

The simulation data includes 5 subjects comprised of a mixture of 5 time courses,

with 284 time points and 5 paired brain networks (shown in Fig. 1), which are generated from "standard" resting-state brain networks to simulate realistic fMRI signals (Damoiseaux et al., 2006). Gaussian noise was added to each time point to give a signal-noise ratio of 4 (6dB). A bias baseline was generated for each time point. The SNR is defined as the equation below:

$$\mathrm{SNR} = \left(\frac{\mathrm{A_s}}{\sigma_\mathrm{n}}\right)^2 = 20\log\left(\frac{\mathrm{A_s}}{\sigma_\mathrm{n}}\right)$$

where $\mathrm{A_s}$ is the amplitude of the signal and σ_n is the standard deviation of the noise.

Figure 1 here

2.2. In vivo clinical data

A dataset used in this study included 58 participants from 3 groups: 20 designated DM (type II diabetes mellitus, 12 females, 8 males, age 60.39 ± 5.18), 20 designated SD (type II diabetes mellitus with sleep disorder, 12 females, 8 males, age 60.27 ± 5.89), and 18 designated HC (health comparison subjects, 11 females, 7 males, age 57.28 ± 4.48). All participants signed informed consent forms approved by the ethics committee of the Dalian University of Technology and Affiliated Zhongshan Hospital of Dalian University.

MRI scanning was performed on a 3-Tesla (3T) MRI scanner (Verio, Siemens, Germany) using a 12-channel phased-array head coil. High-resolution T1-weighted images were acquired using a magnetization-prepared rapid gradient echo (MPRAGE) sequence, with repetition time (TR) = 2530 ms, echo time (TE) = 2.22 ms, flip angle = 7°, matrix size = 224 × 224, field of view (FOV) = 224 × 224 mm, voxel size = 1 × 1 × 1 mm, and slice thickness = 1mm; the scanning time was 5 minutes 28 seconds. Rs-fMRI data were acquired using an echo-planar image (EPI) pulse sequence with parameters as follows: TR = 2000 ms, TE = 30 ms, flip angle = 90◦, FOV = 224 × 224 mm, and matrix = 64 × 64, the scanning time was 8 minutes. Pre-processing was done with DPABI (rfmri.org/dpabi). Functional images were slice-time corrected, realigned for head motion correction, registered into the MNI152 standard space template, rescaled to 3×3×3 mm3 resolution, and smoothed with a FWHM 6 mm Gaussian kernel. In the temporal domain, detrending and a 0.01Hz to 0.1Hz bandpass filter were applied to remove the system interference and abnormal frequency components.

2.3. In 7T HCP Datasets

The performance of our proposed method was also evaluated on the 7T HCP dataset (Human Connectome Project: www.humanconnectome.org). We selected 10 subjects (10 females, 27.6 ± 1.6) with a "minimally preprocessing" procedure (Glasser et al., 2013) including gradient unwarping, motion correction, fieldmap-based EPI distortion correction, brain-boundary-based registration of EPI to structural T1-weighted scan, non-linear registration into MNI152 space, and grand-mean intensity normalization. For details of the data acquisition parameters see (Van Essen et al., 2013).

We did smooth the data with a kernel of FWHM of 8mm with FSL (Smith et al., 2004, https://fsl.fmrib.ox.ac.uk/fsl/fslwiki/), but besides that, no further processing was applied on the data so that preprocessing would not affect the results. The brain mask was generated by average 10 subjects and was used to transfer the 113 x 136 x 113 matrix into a length 408678 vector.

2.4. Spatial-temporal components stability index

ICA, as a well-established method for determining networks of neuronal connectivity, was applied to the fMRI data for the effectiveness as a solution for the problem of blind source separation. If we take brain functional networks as the sources, the noise-free model will be:

$$\mathbf{X} = \mathbf{AS} = \mathbf{a}_1 \circ \mathbf{s}_1 + \cdots + \mathbf{a}_r \circ \mathbf{s}_r + \cdots + \mathbf{a}_R \circ \mathbf{s}_R,$$

where $\mathbf{S} \in \mathbb{R}^{R\times M}$ is the source component, $\mathbf{A} \in \mathbb{R}^{N\times R}$ is the mixing matrix, and $\mathbf{X} \in \mathbb{R}^{N\times M}$ is the observation.

The stability of spatial and temporal components was evaluated by using a hierarchical cluster analysis of tensors via the tensor clustering toolbox (Himberg et al., 2004; Hu et al., 2019). In the toolbox, a rank-1 matrix $\mathbf{E}^r$ **was** calculated by the outer-product of r^{th} independent component's spatial map $\mathbf{a}_r$ and corresponding time course $\mathbf{s}_r$. The clustering quality I_q and similarity matrix of $\mathbf{S}_{ij}$ in Tensor Clustering were defined as below:

$$\mathbf{S}_{ij} = \sum(\mathbf{E}^i \odot \mathbf{E}^j) = \sum\left[(\mathbf{a}_i \circ \mathbf{s}_i) \cdot (\mathbf{a}_j \circ \mathbf{s}_j)\right],$$

$$I_q(r) = \bar{S}(r)_{in} - \bar{S}(r)_{ex},$$

where $\bar{S}(r)_{in}$ and $\bar{S}(r)_{ex}$ respectively stand for the mean intra-class and inter-class similarity of r^{th} cluster.

After tensor clustering, the rank-1 matrices could be used to stand for the reliability of each spatial-temporal component within the specific MO. That is to say, each single IC will have its own clustering quality index, i.e. I_q.

2.5. Consistent component stability index

The proposed CoCA method requires a range of MOs, over which the ICA algorithm could run for multiple times, for each MO. The "ideal" number of runs varies substantially in different literatures (Groppe et al., 2009; Meinecke et al., 2002). We recommend the number of runs for single MO larger than 50, which we believe is an acceptable compromise between computation cost (using CPU methods, which is the most common) and accuracy. Multiple MOs are required to measure the consistency of each component, which allow visual comparison between MOs and components and allow selection of both sets of consistent components and the optimal model order.

The flowchart of CoCA is demonstrated in Fig. 2. The process includes two stages: stage one focuses on single MO assessment to determine a reasonable MO range; stage two implements the core steps of CoCA - calculating the component consistency indices

and doing consistency assessments across model order. Stage one has already been well understood, as it is a standard part of ICA analysis. Stage two is relatively novel, and is summarized with the following detailed description. If MO ranges from 2 to K, there will be a $k \in [2, K]$ which yields the best performance among the tensor clustering results, and denotes that these k ICs will have consistent quality for any further analysis. The consistency of components in optimal MO across all MOs was evaluated with the procedure below for all $k \in [2, K]$:

1) Recover the time-courses $\mathbf{T_c} \in \mathbb{R}^{N\times k}$ from the mixing matrix $\mathbf{A} = \mathbf{VW^{-1}}$ ($\mathbf{V}$ is the orthonormal matrix in PCA for dimension reduction);

2) Recover the spatial maps $\mathbf{S_m} \in \mathbb{R}^{k\times M}$ from the source matrix $\mathbf{S} = \mathbf{WV^T X}$;

3) Calculate the correlation coefficients of the spatial-temporal components (combined $\mathbf{T_c}$ and $\mathbf{S_m}$) between MO k and other MO 2 to MO R, which then will result in a mapped correlation coefficient matrix $\mathbf{C_{map}} \in \mathbb{R}^{R\times R\times k}$;

4) Pair each MO component with one and only one of the k components in MO k based on the maximum correlation coefficient, forming a binary index matrix $\mathbf{I_{hc}} \in \mathbb{R}^{\mathbf{R\times k}}$;

5) Based on the $\mathbf{I_{hc}}$ indexing out two matrixes I_q and r_{max} from tensor clustering results and correlation coefficients ergodic results;

6) Assess consistent quality (C_q) based on I_q and r_{max} in the two phases, for MO less than and greater than MO k.

The consistency quality (C_q, take r_{max} as an example) is based on the I_q and r_{max}, combining the appearance of the components to address the consistency of one specific component. For phase one, as MO is less than k, there are not enough paired IC's for all k components. Because certain consistent components will appear over the range of 2 to k while some will not. In contrast to the consistent components, we define those inconsistent components as 'broken' ICs. A 'broken' IC has the tendency to appear and disappear in the paired components, which helps us to set up penalty terms by the number (L_b) and frequencies (L_f) of being absent since the first time it appears in the model. High values of these terms would indicate inconsistent ICs. The definition is shown below:

$$C_q = \beta \bar{r_i}$$

$$\beta = 1 - \frac{L_b L_f}{k^2},$$

where β is the punishment parameter, $\bar{r_i}$ $(i = 1,2,\cdots,k)$ is the average correlation coefficient of all the component paired with the i^{th} IC in MO k, L_b, L_f stands for the number and frequencies of those 'broken' ICs. As for phase two, C_q is easier to assess, since there are no absent IC's. Here, the standard deviation of the slope of r_i, which represents the fluctuation of r, is subtracted as the punishment. Cq is therefore defined as below:

$$C_q = \bar{r}_i - \mathrm{std}(r_{i,j} - r_{i,j-1}), j = k+1, \cdots, R.$$

Figure 2 here

3. Results

3.1. Simulated data

For the sake of generality, both FastICA and InfomaxICA were both run 50 times. The proposed scheme was used to obtain the optimal MO and detect consistent components. According to the tensor clustering results, the optimal MO was determined, and further stability and consistency analyses are shown in Fig. 3 and Fig. 4. For the FastICA results, the 5 ground truth components stand out at the optimal MO = 7, and the consistency analysis demonstrates exactly how the noise signal corrupts the components with increasing MO. As for the InfomaxICA result, the rank-1 spatial-temporal matrix tensor clustering reveals the decreasing I_q index for noise components. In the InfomaxICA algorithm analysis, the noise signal looks somewhat consistent for the rank-1 matrix, based on the spatial maps and time courses through the different MOs; however, the consistent I_q does not conceal the fact that the noise is unstable. This shows that such noise has the potential to give rise to consistent components, especially when the InfomaxICA algorithm works to maximize the information from data. The consistent performance contrast between the source signal and noise is clear and bounded - the stubborn noise and artifacts in real fMRI data can highly exhibit the same nature. In this case, further physiological plausibility analyses would be needed to reveal the difference.

Figure 3 here

Figure 4 here

3.2. In vivo clinical data

Stability analysis for consistent components

The convergence of ICA (Fig. 5a) results shows that when model order (MO) is over 30, the convergence drops dramatically. Based on the rank-1 matrix tensor clustering quality index I_q (Fig. 5b), all averaged I_q values were larger than 0.8 before MO = 30, which set a lower bound for the MO range (less than 25) with good performance in 50 runs.

Figure 5 here

The results of the tensor clustering are displayed using 2D-projection visualization, as shown in Fig. 6. It shows clearly that some connection between clusters appears, and the density of some clusters decreases as the MO is increased. What's more interesting

is that some badly shaped and overlapped clusters in MO 25 perform better in MO 30 (IC#19 and IC#25 in MO 25). With the criteria mentioned above, MO 21 was chosen to be the optimal, resulting in a set of 21 ICs with consistent quality. Several commonly used information criteria were implemented to represent its irrational suggestion, and the estimation results of AIC, KIC and MDL indicated that the optimal model order goes to 11, 9 and 2. It is obvious that ICs decomposed in these so-called optimal model orders are basically inconsistent (Fig. 7).

Figure 6 here

Figure 7 here

The correlation coefficients of the paired ICs in MO 21 (Fig. 7a) indicate that not every IC has a good consistency, as some may be 'broken'. The reason could be that the increasing number of the MO brings a larger amount of information into the ICA iterations, which could induce instability in some ICs. The C_q based on correlation coefficients for every IC in MO 21 (Fig. 7b) shows that consistent components (CC) could be clearly addressed with a higher mean C_q above 0.8 like CC#1, CC#2, CC#3.

Figure 8 here

In Fig.8, I_q values are obviously higher in phase one, because the ICs with MO less than 21 are in good condition, as seen from the tensor clustering results shown in Fig. 6. In phase two, some ICs with 'unpleasant' I_q values emerge as a prediction of instability. Then, we could tell the C_q, based on I_q, should be larger than 0.9 as a threshold for consistency, namely, CC#1, CC#2, CC#3 and some other ICs stand out. So far, correlation coefficient and I_q based on C_q are equally important; one stands for the validity of phase one and the other of phase two. It is obvious that correlation coefficients are more sensitive to larger differences than smaller ones (our interest is to exclude the inconsistent ICs, so the Fisher z transformation is not applied to differ higher correlation), which are often detected in phase one. In contrast, the index I_q refers to the clustering result of components, and the performance would be good if the estimated model order is less than the ideal one. Empirically and theoretically, I_q varies more easily when MO is higher, thus it is more sensitive in phase two. However, the final decision cannot be made without combining both of them. In this study, IC#1, IC#2, IC#3, IC#5, IC#7, IC#8, IC#12, and IC#19 are picked out as CCs fulfilling the requirement that C_q values are larger than the threshold of 0.9 for I_q and 0.8 for the correlation coefficients.

Spatial map plausibility and statistical analyses

Group ICA was applied in this study, and the first time PCA was employed for single subject data to reduce dimensionality, with the criteria of retaining enough

components to explain 95% of the variance. Then the second time PCA was employed for model order determination. After ICA decomposition, time-courses of each subject were recovered, and the Fourier transform was applied to measure the amplitude of low-frequency fluctuation (ALFF, Di et al., 2012). Then, an overall 3 x 1 ANOVA was used to examine statistical significance with the p-value less than 0.05. Meanwhile, the spatial maps were recovered and converted to Z-values (by dividing by the standard deviation of the source) and thresholded at $|Z| > 2.3$ for display.

After excluding some ICs with irrational spatial maps (e.g. a lower correlation coefficient with 'standard' resting networks or a noisy distribution with excessive scattered clusters) or uncorrectable p-value, among the qualified results, IC#2 ($p = 0.02$) and IC#5 ($p = 0.0159$), were picked out for the demonstration. The spatial maps of the two ICs are displayed in Fig. 9. However, the multiple comparison results showed that major effects were from the difference between two diabetes mellitus groups and the HC group. Both the Calcarine area in IC#2, and the Middle Frontal and Inferior Parietal areas in IC#5, have previously been found associated with the changes in vision and cognition. Furthermore, the Montreal Cognitive Assessment (MoCA) was performed for each subject. The correlation between ALFF (IC#5, Middle Frontal area) and MoCA index was shown in Fig.10. The positive correlation between MoCA and the mean value of ALFF was found in the Middle Frontal area in IC#5 for both SD and DM groups. However, only the DM group showed a significant result with a p-value less than 0.05.

Figure 9 here

Figure 10 here

3.3. In 7T HCP Datasets

The 7T HCP datasets are high-resolution fMRI datasets and only included healthy subjects. It is helpful to evaluate the performance of CoCA by focusing on the stability or consistency of rest-state networks. Considering the memory and computing efficacy, we adjusted the ratio of dimensionality reduction in the first PCA from 95% to 80% of explained variance and the second PCA result was a big matrix sized as 408678*912. To compare with a traditional fixed model order ICA, the model order estimation algorithm AIC, KIC, and MDL were used to estimate the second PCA result, and the suggesting model orders were AIC for 25, KIC for 10, and MDL for 1. The estimation results were not coherent and the later consistency analyses proved our method was more rational than such information-theoretic criteria. Compared to the clinical datasets, we assessed the 7T HCP dataset in a more comprehensive and perspective way.

Based on the tensor clustering results listed in **Fig. 11**, we selected the MO 20 as the optimal order, and the model order ranged from 10 to 30. The consistent analysis results based on correlation coefficients and I_q were separately shown in **Fig. 12** and **Fig. 13**. We could find out that several ICs, from IC#4 to IC#10, have represented a very good consistency. IC#1, IC#2, IC#3, IC#14, IC#15, and IC#19, these components

with a C_q higher than 0.8 could also be regarded as the consistent components. Therefore, it will be more comprehensive to address the variation of this metric by giving some examples. Some inconsistent components here, IC#11, IC#12, IC#13, and so on, have a tragic dropdown in MO 23. So, we recovered the spatial maps of IC#11 and IC#12 from MO 20 and their paired components IC#22 and IC#14 in MO 23 for comparison (**Fig. 14**). All the spatial maps were scaled with z-score transformation and thresholded at $|Z| > 1.6$. According to **Fig. 13**, it was noticeable that the differences between spatial maps were coherent with the differences between the correlation coefficients. For IC#11, its correlation difference between MO 20 and MO 23 (IC#22 in MO 23) was much smaller than IC#12, and so does the variation of the spatial maps.

To make the result much clearer and easier to follow, we increased the MO range to 50 on optimal model order 20 and 23 (**Fig. 15**). Meanwhile, by separating the spatial-temporal matrix into spatial maps and temporal courses, we could have a perceptual perspective in understanding why the consistent analysis is crucial and important. In Fig. 14, the ICs with strong consistency might persist along with model order (IC#5, in MO 20 when no specification) and some could also be slightly changed (IC#9 and IC#19). The consistency, it required the spatial maps and temporal courses both kept on the same paving. Because corruption happened in any one of them would result in poor consistency. On the other hand, some inconsistent ICs may become more consistent when MO increasing brought more information, and their spatial maps or temporal courses would not always stay the same or simply fractionate. Actually, they evolved along with the MO until enough information served its consistency or stability (IC#2 and IC#3). However, IC#14 in MO 23 contained more structural noise components compared to IC#12 in MO 20 as shown in Fig. 14, but its spatial maps only were incidental or unstable results, because we could find out that it quickly evolved after several model orders. The consistency of spatial maps or temporal courses might not keep in the same pave, but well-performed ICs always scored high in both perspectives as shown in Fig. 15. The above results indicated that the CoCA could contribute in giving more confidence in the ICA decomposition results, no matter under what kind of applications, using ideal model order supported by prior knowledge or estimated by any methods.

Figure 11-15 here

4. Discussion

The consistency of independent components over model orders has not received adequate study as an assessment factor to establish the stability of the ICA decomposition. In (Groves et al., 2012; Ray et al., 2013), a similar scheme was used for reproducibility test, however, they chose only two dimensions to pair components. Our method not only evaluates the consistency across all model orders, but also quantifies it with C_q index. Our protocol can also bcre used to distinguish cases of components

splitting as dimensionality increases, cases of new components appearing carrying additional information, and stubborn structural noise components. Along with the model range detection for consistency, evolving components could be detected through correlation coefficient changes; for example, in the in vivo data, IC#10 had a clear up-down gradient fluctuation. C_q, based on I_q, can be utilized to identity the clustering results, and is an interesting index to show when one component splits or two components merge as the MO increases. Our method also has a potential to trace ICA decomposition progress and provide a metric for interrupting ICA with a priori knowledge.

In our vivo clinical data test, two chosen ICs were typical brain regions that have been found in many previous studies(Cui et al., 2014; Hu et al., 2019; Wang et al., 2014). There were additional ICs that could be used to represent the significant difference between diabetes mellitus groups and healthy groups, but we presented only these two for clarity. As for those inconsistent components in the result, not all of them are noise, as we had originally thought (for example, scattered clusters, gaussian noise throughout the brain, etc.) Empirically, we would expect that the dominant components would be brain networks. However, the most common, and disturbing, situation encountered in the ICA results are the presence of compound components (i.e. the brain network we are interested combined with noise components). The independence constraint only requires that consistent components (e.g., IC#1 and IC#2) be exactly that - independent components. Our proposed method will perfectly do its job detecting consistent components and has no bias for or against any IC, whether it is signal or noise. For stubborn structural noise components, there is a highly chance that they may become a single IC, or part of an IC that consistently exists over model orders, while fragile and vulnerable noise, or signal/noise mixed components, are more sensitive to model order. Our proposed method as a stability or reproducibility analyses method, the main target is to distinguish consistent and stable components from those inconsistent ones with consistency metrics.

Some ICA applications use much higher MO in decomposition (Abou-Elseoud et al., 2010; Allen et al., 2011; Groves et al., 2012; Iraji et al., 2019; Kiviniemi et al., 2009; Li et al., 2007; Wei et al., 2017; Ystad et al., 2010). The reproducibility, stability or consistency concerns for higher MO cannot be fulfilled by doing a comparison between one lower and one higher MO or simply check the existence of some key components. No matter how fragile the ICs are, the ICA tends to separate statistically significant independent sources with effectively i.i.d. samples from the dependent data(Li et al., 2007). And some vital or interesting components like the subnetworks of DMN(Hu et al., 2016), may only be distinguished when the MO is high enough. Under such circumstances, a well-performed, objective stability analyses is critical. Our proposed scheme can help to evaluate any potential interesting component over a range of MO to determine its stability, and how it evolves with increasing model order, as the ICs

split and merged.

Another key factor of the reliability method is the 'stable' index threshold (Artoni et al., 2014; Remes et al., 2011). Usually, extracted components and coefficients of adaptive iteration algorithms (e.g., ICA) run the risk of being unstable because of model order selection. So reproducibility or stable analyses increase the confidence in the results of a study. But the appropriate threshold for these indices may be different in various applications. To address this issue, the proposed method, CoCA, takes into consideration that the index of stability should involve not only the single MO but also a certain MO range. Moreover, CoCA provides the index of all paired ICs between MO, which means the correlation coefficient and I_q of all ICs are traceable. Any ambiguous ICs can be identified via visual inspection or can be subjected to further analysis to decide if it should be kept or ruled out.

In sum, the CoCA is a consistency analysis based on correlation coefficients and tensor clustering indices, which combines the ICASSO and rank-1 spatial-temporal matrix, deriving from a cross-MO ergodic strategy. Such a strategy is potentially suitable for any other adaptive iteration algorithm to evaluate their stability. Our software is available in https://github.com/WeiZhao04/CoCA.git.

CRediT author statement

Wei Zhao: Conceptualization, Software, Data curation, Writing - Original Draft. **Huanjie Li:** Conceptualization, Methodology. **Guoqiang Hu:** Software. **Yuxing Hao:** Validation. **Qing Zhang:** Resources. **Jianlin Wu:** Resources. **Blaise B.Frederick:** Writing - Review & Editing, Supervision. **Fengyu Cong:** Supervision, Funding acquisition, Project administration.

Declarations of interest: none

Declaration of Competing Interest

The authors declare that the research was conducted in the absence of any commercial or financial relationships that could be construed as a potential conflict of interest.

Acknowledgements

This work was supported by National Natural Science Foundation of China (Grant No. 91748105 & 81601484), and National Foundation in China (No. JCKY 2019110B009 & 2020-JCJQ-JJ-252), and the scholarships from China Scholarship Council (Nos. 202006060130), and the Fundamental Research Funds for the Central Universities [DUT2019, DUT20LAB303] in Dalian University of Technology in China.

Appendix

Time-course and spatial map recovery

Group ICA is used in this study, and the first level PCA is applied to the pre-processed data of each subject, and then temporally concatenated into a group-wise dataset. Then, based on the basic assumption of temporal concatenated Group ICA, all subjects share the same spatial maps but different mixing matrices as below:

$$\mathbf{X}^{(i)} = \mathbf{A}^{(i)}\mathbf{S}$$
$$\mathbf{Z}^{(i)} = \mathbf{V}^{T(i)}\mathbf{X}^{(i)} = \mathbf{V}^{T(i)}\mathbf{A}^{(i)}\mathbf{S}$$

where $i = 1,2,\cdots,P$, denotes the i^{th} subject in a total of P subjects, and $\mathbf{V}^{T(i)}$ is the transformation matrix for dimension reduction. After temporal concatenation, a second level PCA is applied for model estimation reduction.

$$\mathbf{Z_G} = \mathbf{V_G}\mathbf{D_G}\mathbf{S_G}$$
$$\mathbf{D_G} = \begin{bmatrix} \mathbf{V}^{T(1)}\mathbf{A}^{(1)} & \cdots & \mathbf{0} \\ \vdots & \ddots & \vdots \\ \mathbf{0} & \cdots & \mathbf{V}^{T(P)}\mathbf{A}^{(P)} \end{bmatrix},\ \mathbf{S_G} = \begin{bmatrix} \mathbf{S} \\ \vdots \\ \mathbf{S} \end{bmatrix},$$

where $\mathbf{Z_G} \in \mathbb{R}^{\mathbf{NP}\times\mathbf{M}}$ and $\mathbf{V_G} \in \mathbb{R}^{\mathbf{NP}\times\mathbf{NP}}$ are the group-wise observations and group orthonormal matrix. $\mathbf{D_G}$ is a block diagonal matrix consisting of $\mathbf{V}^{T(i)}\mathbf{A}^{(i)}$.

Finally, $\mathbf{Z_G}$ was inputted into the ICA model and the formulation could be denoted using the unmixing matrix $\mathbf{W_G}$ as follow:

$$\mathbf{Y_G} = \mathbf{W_G}\mathbf{Z_G} = \mathbf{W_G}\mathbf{V_G^T}\mathbf{D_G}\mathbf{S_G}$$

where $\mathbf{Y_G}$ is the estimation of sources. As for the noise-free model, it should equal to $\mathbf{S_G}$ with the polarity and variance indeterminacy discarded already. If we take the stack of data into consideration, then $\mathbf{W_G}\mathbf{V_G}$ can be divided into blocks for each subject. The b_i denotes the block of the i^{th} subject as follow:

$$\left(\mathbf{W_G}\mathbf{V_G^T}\right)_{b_i}\mathbf{V}^{T(i)}\mathbf{A}^{(i)} = \mathbf{I},$$

And the time-course of each subject can be recovered as the formula below:

$$A^{(i)} = \left(\left(W_G V_G^T\right)_{b_i} V^{T(i)}\right)^{-1}.$$

References

Abou-Elseoud, A., Starck, T., Remes, J., Nikkinen, J., Tervonen, O., Kiviniemi, V., 2010. The effect of model order selection in group PICA. Hum. Brain Mapp. 31, 1207–1216. https://doi.org/10.1002/hbm.20929

Allen, E.A., Erhardt, E.B., Damaraju, E., Gruner, W., Segall, J.M., Silva, R.F., Havlicek, M., Rachakonda, S., Fries, J., Kalyanam, R., Michael, A.M., Caprihan, A., Turner, J.A., Eichele, T., Adelsheim, S., Bryan, A.D., Bustillo, J., Clark, V.P., Feldstein Ewing, S.W., Filbey, F., Ford, C.C., Hutchison, K., Jung, R.E., Kiehl, K.A., Kodituwakku, P., Komesu, Y.M., Mayer, A.R., Pearlson, G.D., Phillips, J.P., Sadek, J.R., Stevens, M., Teuscher, U., Thoma, R.J., Calhoun, V.D., 2011. A Baseline for the Multivariate Comparison of Resting-State Networks. Front. Syst. Neurosci. 5. https://doi.org/10.3389/fnsys.2011.00002

Artoni, F., Menicucci, D., Delorme, A., Makeig, S., Micera, S., 2014. RELICA: A method for estimating the reliability of independent components. Neuroimage 103, 391–400. https://doi.org/10.1016/j.neuroimage.2014.09.010

Calhoun, V.D., Adali, T., Pearlson, G.D., Pekar, J.J., 2001. A method for making group inferences from functional MRI data using independent component analysis. Hum. Brain Mapp. 14, 140–151. https://doi.org/10.1002/hbm.1048

Celone, K. a, Calhoun, V.D., Dickerson, B.C., Atri, A., Chua, E.F., Miller, S.L., DePeau, K., Rentz, D.M., Selkoe, D.J., Blacker, D., Albert, M.S., Sperling, R. a, 2006. Alterations in memory networks in mild cognitive impairment and Alzheimer's disease: an independent component analysis. J. Neurosci. 26, 10222–10231. https://doi.org/10.1523/JNEUROSCI.2250-06.2006

Cong, F., He, Z., Hämäläinen, J., Leppänen, P.H.T., Lyytinen, H., Cichocki, A., Ristaniemi, T., 2013. Validating rationale of group-level component analysis based on estimating number of sources in EEG through model order selection. J. Neurosci. Methods 212, 165–172. https://doi.org/10.1016/j.jneumeth.2012.09.029

Cong, F., Lin, Q.H., Astikainen, P., Ristaniemi, T., 2014. How to validate similarity in linear transform models of event-related potentials between experimental conditions? J. Neurosci. Methods 236, 76–85. https://doi.org/10.1016/j.jneumeth.2014.08.018

Cui, Y., Jiao, Y., Chen, Y., Wang, K., Gao, B., Wen, S., Ju, S., Teng, G., 2014. Altered Spontaneous Brain Activity in Type 2 Diabetes : A Resting-State Functional MRI Study 63, 749–760. https://doi.org/10.2337/db13-0519

Damoiseaux, J.S., Rombouts, S.A.R.B., Barkhof, F., Scheltens, P., Stam, C.J., Smith, S.M., Beckmann, C.F., 2006. Consistent resting-state networks across healthy subjects. Proc. Natl. Acad. Sci. U. S. A. 103, 13848–53. https://doi.org/10.1073/pnas.0601417103

Di, X., Zhu, S., Jin, H., Wang, P., Ye, Z., Zhou, K., Zhuo, Y., Rao, H., 2012. Altered Resting Brain Function and Structure in Professional Badminton Players. Brain Connect. 2, 225–233. https://doi.org/10.1089/brain.2011.0050

Flandin, G., Friston, K., 2008. Statistical parametric mapping (SPM). Scholarpedia 3, 6232. https://doi.org/10.4249/scholarpedia.6232

Friston, K.J., Harrison, L., Penny, W., 2003. Dynamic causal modelling. Neuroimage 19, 1273–1302. https://doi.org/10.1016/S1053-8119(03)00202-7

Griffanti, L., Salimi-Khorshidi, G., Beckmann, C.F., Auerbach, E.J., Douaud, G., Sexton, C.E., Zsoldos, E., Ebmeier, K.P., Filippini, N., Mackay, C.E., Moeller, S., Xu, J., Yacoub, E., Baselli, G., Ugurbil, K., Miller, K.L., Smith, S.M., 2014.

ICA-based artefact removal and accelerated fMRI acquisition for improved resting state network imaging. Neuroimage 95, 232–247. https://doi.org/10.1016/j.neuroimage.2014.03.034

Groppe, D.M., Makeig, S., Kutas, M., 2009. Identifying reliable independent components via split-half comparisons. Neuroimage 45, 1199–1211. https://doi.org/10.1016/j.neuroimage.2008.12.038

Groves, A.R., Smith, S.M., Fjell, A.M., Tamnes, C.K., Walhovd, K.B., Douaud, G., Woolrich, M.W., Westlye, L.T., 2012. Benefits of multi-modal fusion analysis on a large-scale dataset: Life-span patterns of inter-subject variability in cortical morphometry and white matter microstructure. Neuroimage 63, 365–380. https://doi.org/10.1016/j.neuroimage.2012.06.038

Himberg, J., Hyvärinen, A., Esposito, F., 2004. Validating the independent components of neuroimaging time series via clustering and visualization. Neuroimage 22, 1214–1222. https://doi.org/10.1016/j.neuroimage.2004.03.027

Hu, G., Zhang, Q., Waters, A.B., Li, H., Zhang, C., Wu, J., Cong, F., Nickerson, L.D., 2019. Tensor clustering on outer-product of coefficient and component matrices of independent component analysis for reliable functional magnetic resonance imaging data decomposition. J. Neurosci. Methods 325, 108359. https://doi.org/10.1016/j.jneumeth.2019.108359

Hu, Y., Wang, J., Li, C., Wang, Y.S., Yang, Z., Zuo, X.N., 2016. Segregation between the parietal memory network and the default mode network: effects of spatial smoothing and model order in ICA. Sci. Bull. 61, 1844–1854. https://doi.org/10.1007/s11434-016-1202-z

Hyvärinen, A., 1999. Fast and robust fixed-point algorithms for independent component analysis. IEEE Trans. neural networks 10, 626–34. https://doi.org/10.1109/72.761722

Iraji, A., Faghiri, A., Lewis, N., Fu, Z., DeRamus, T., Qi, S., Rachakonda, S., Du, Y., Calhoun, V., 2019. Ultra-high-order ICA: An exploration of highly-resolved data-driven representation of intrinsic connectivity networks (Sparse ICNs), in: VanDeVille, D and Papadakis, M and Lu, YM (Ed.), WAVELETS AND SPARSITY XVIII, Proceedings of SPIE. SPIE-INT SOC OPTICAL ENGINEERING, 1000 20TH ST, PO BOX 10, BELLINGHAM, WA 98227-0010 USA. https://doi.org/10.1117/12.2530106

J.Sejnowski, A.B. and T., 1995. Information-Maximization Approach to Blind Separation and Blind Deconvolution. Technology 1159, 1129–1159.

Kiviniemi, V., Starck, T., Remes, J., Long, X., Nikkinen, J., Haapea, M., Veijola, J., Moilanen, I., Isohanni, M., Zang, Y., Tervonen, O., 2009. Functional segmentation of the brain cortex using high model order group PICA. Hum. Brain Mapp. 30, 3865–3886. https://doi.org/10.1002/hbm.20813

Levin-Schwartz, Y., Calhoun, V.D., Adali, T., 2017. Quantifying the Interaction and Contribution of Multiple Datasets in Fusion: Application to the Detection of Schizophrenia. IEEE Trans. Med. Imaging 36, 1385–1395. https://doi.org/10.1109/TMI.2017.2678483

Li, Y.O., Adali, T., Calhoun, V.D., 2007. Estimating the number of independent components for functional magnetic resonance imaging data. Hum. Brain Mapp. 28, 1251–1266. https://doi.org/10.1002/hbm.20359

Meindl, T., Teipel, S., Elmouden, R., Mueller, S., Koch, W., Dietrich, O., Coates, U., Reiser, M., Glaser, C., 2010. Test-retest reproducibility of the default-mode network in healthy individuals. Hum. Brain Mapp. 31, 237–246. https://doi.org/10.1002/hbm.20860

Meinecke, F., Ziehe, A., Kawanabe, M., Müller, K.R., 2002. A resampling approach to estimate the stability of one-dimensional or multidimensional independent components. IEEE Trans. Biomed. Eng. 49, 1514–1525. https://doi.org/10.1109/TBME.2002.805480

Pruim, R.H.R., Mennes, M., van Rooij, D., Llera, A., Buitelaar, J.K., Beckmann, C.F., 2015. ICA-AROMA: A robust ICA-based strategy for removing motion artifacts from fMRI data. Neuroimage 112, 267–277. https://doi.org/10.1016/j.neuroimage.2015.02.064

Ray, K.L., McKay, D.R., Fox, P.M., Riedel, M.C., Uecker, A.M., Beckmann, C.F., Smith, S.M., Fox, P.T., Laird, A.R., 2013. ICA model order selection of task co-activation networks. Front. Neurosci. 7, 1–12. https://doi.org/10.3389/fnins.2013.00237

Remes, J.J., Starck, T., Nikkinen, J., Ollila, E., Beckmann, C.F., Tervonen, O., Kiviniemi, V., Silven, O., 2011. Effects of repeatability measures on results of fMRI sICA: A study on simulated and real resting-state effects. Neuroimage 56, 554–569. https://doi.org/10.1016/j.neuroimage.2010.04.268

Smith, S.M., Jenkinson, M., Woolrich, M.W., Beckmann, C.F., Behrens, T.E.J., Johansen-Berg, H., Bannister, P.R., De Luca, M., Drobnjak, I., Flitney, D.E., Niazy, R.K., Saunders, J., Vickers, J., Zhang, Y., De Stefano, N., Brady, J.M., Matthews, P.M., 2004. Advances in functional and structural MR image analysis and implementation as FSL. Neuroimage 23, 208–219. https://doi.org/10.1016/j.neuroimage.2004.07.051

Van Essen, D.C., Smith, S.M., Barch, D.M., Behrens, T.E.J., Yacoub, E., Ugurbil, K., 2013. The WU-Minn Human Connectome Project: An overview. Neuroimage 80, 62–79. https://doi.org/10.1016/j.neuroimage.2013.05.041

Wang, C., Fu, K., Liu, H., Xing, F., Zhang, S., 2014. Spontaneous Brain Activity in Type 2 Diabetics Revealed by Amplitude of Low-Frequency Fluctuations and Its Association with Diabetic Vascular Disease : A Resting- State fMRI Study 9, 1–12. https://doi.org/10.1371/journal.pone.0108883

Wei, L., Hu, X., Zhu, Y., Yuan, Y., Liu, W., Chen, H., 2017. Aberrant Intra- and Internetwork Functional Connectivity in Depressed Parkinson's Disease. Sci. Rep. 7, 1–12. https://doi.org/10.1038/s41598-017-02127-y

Wisner, K.M., Atluri, G., Lim, K.O., MacDonald, A.W., 2013. Neurometrics of intrinsic connectivity networks at rest using fMRI: Retest reliability and cross-validation using a meta-level method. Neuroimage 76, 236–251. https://doi.org/10.1016/j.neuroimage.2013.02.066

Ystad, M., Eichele, T., Lundervold, A.J., Lundervold, A., 2010. Subcortical functional connectivity and verbal episodic memory in healthy elderly-A resting state fMRI study. Neuroimage 52, 379–388. https://doi.org/10.1016/j.neuroimage.2010.03.062

Fig. 1. (a) Five source maps are created from the resting state network. (b) Five timecourses with 284 points are shown as specific colors to corresponding source maps.

Fig. 2. The flowchart of CoCA. (A) The progress of model order range determination. (B) The indexes calculation and consistence analysis progress.

Fig. 3. The results and index figures of FastICA. (a) The tensor clustering result of MO = 7 over 50 runs. Consistent components (in this case 1-5) are compact in this space – the large spatial extent of components 6 and 7 show that their values are not highly consistent. (b) Correlation coefficients paired results (c) Rank-1 components index paired results. (d) Consistence index of correlation coefficients. (e) Consistence index of I_q index.

Fig. 4. The results and index figures of InfomaxICA. (a) The tensor clustering results for MO = 7 over 50 runs. Consistent components (in this case 1-5) are compact in this space – the large spatial extent of components 6 and 7 show that their values are not highly consistent. (b) Correlation coefficients paired results (c) Rank-1 components index of paired results. (d) Consistence index of correlation coefficients. (e) Consistence index of I_q index.

Fig. 5. (a) Number of convergences runs in a total of 50 runs from model order 2-50 and (b) the tensor clustering result of the spatial-temporal rank-1 matrix in the same range.

Fig. 6. Visualization for the tensor clustering result in MO 10, MO 15, MO18, MO 21, MO 25 and MO 30. Blue numbers label the extracted ICs, and the black dots (ICs) are clustered within convex hulls. And the centroid is highlighted using blue circle. Red lines connected dots denotes the similarity of them.

Fig. 7. (a) Paired correlation coefficient results for all IC's found in the optimal MO 21 with components found in model orders over the range from 2-30. Model order increases from left to right. Some components are consistent over all runs–IC#2 and IC#11 appear at MO 2 and persist over all model orders. IC #s 5, 8, 14, 16, 20, and 21 appear in some lower order fits, disappear with increasing model order, and then reappear and persist. Component 18 does not appear until MO 21. The black vertical line shows MO 21 on the y axis–all correlation coefficients are 1 along this line. (b) Consistence quality coefficient in MO 21 address the reliability for each IC. It is clear that there is no Cq for IC#18 in phase one because it's a new IC just appeared since MO 21.

Fig. 8. (a) I_q paired result in optimal MO 21 divided by the black line as the boundary of phase one and phase two. (b) Consistency quality coefficients in MO 21 address the reliability for each IC.

Fig. 9. Spatial maps of IC#2 and IC#5 results (ALFF) in MO#21. Calcarine area in IC#2

and Middle Frontal and Inferior Parietal areas in IC#5.

Fig. 10. Tow groups showed positive correlation between MoCA and ALFF of Middle Frontal area in IC#5, and DM is significant with a p-value lower than 0.05.

Fig. 11. Visualization for the tensor clustering result in MO 15, MO 17, MO 20, and MO 23. Blue numbers label the extracted ICs, and the black dots (ICs) are clustered within convex hulls. And the centroid is highlighted using blue circle. Red lines connected dots denotes the similarity of them.

Fig. 12. (a) Paired correlation coefficient results for all IC's found in the optimal MO 20 with components found in model orders over the range from 10-30. Model order increases from left to right. The black vertical line shows MO 20 on the y axis–all correlation coefficients are 1 along this line. (b) Consistence quality coefficient in MO 20 address the reliability for each IC.

Fig. 13. (a) I_q paired result in optimal MO 20 divided by the black line as the boundary of phase one and phase two. (b) Consistency quality coefficients in MO 20 address the reliability for each IC.

Fig. 14. Spatial maps of IC#11 and IC#12 in MO 20 ICA and their paired components IC#22 and IC#14 in MO 23. The spatial maps were scaled with z-score transformation and thresholded at $|Z|<1.6$.

Fig. 15. Paired correlation coefficient results of spatial maps for all IC's found in the optimal MO 20 (a) and in MO 23 (b) with components found in model orders over the range from 10-50. Paired correlation coefficient results of temporal courses for all IC's found in the optimal MO 20 (c) and MO 23 (d) with components found in model orders over the range from 10-50.

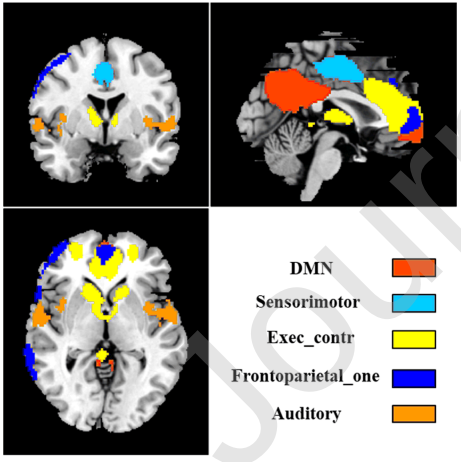

(a) Spatial Maps

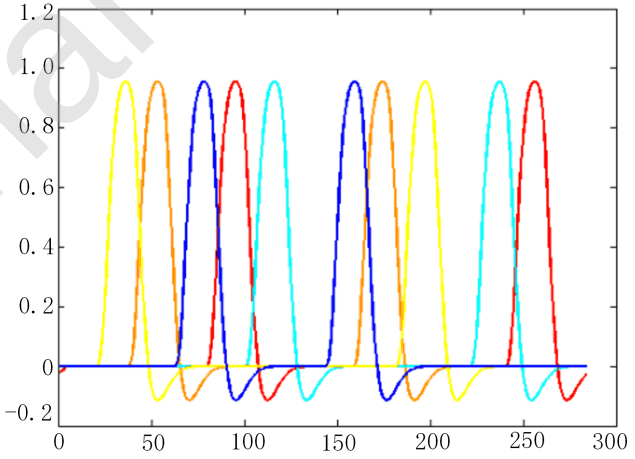

(b) Temporal Courses

Fig. 1. (a) Five source maps are created from the resting state network. (b) Five timecourses with 284 points are shown as specific colors to corresponding source maps.

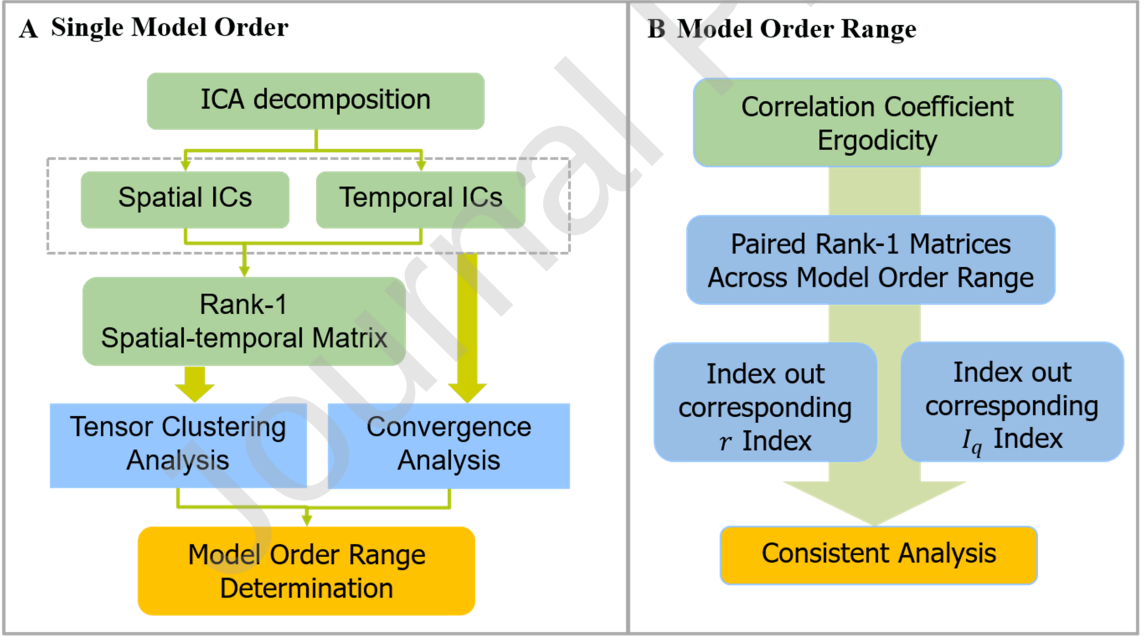

Fig. 2. The flowchart of CoCA. (A) The progress of model order range determination. (B) The indexes calculation and consistence analysis progress.

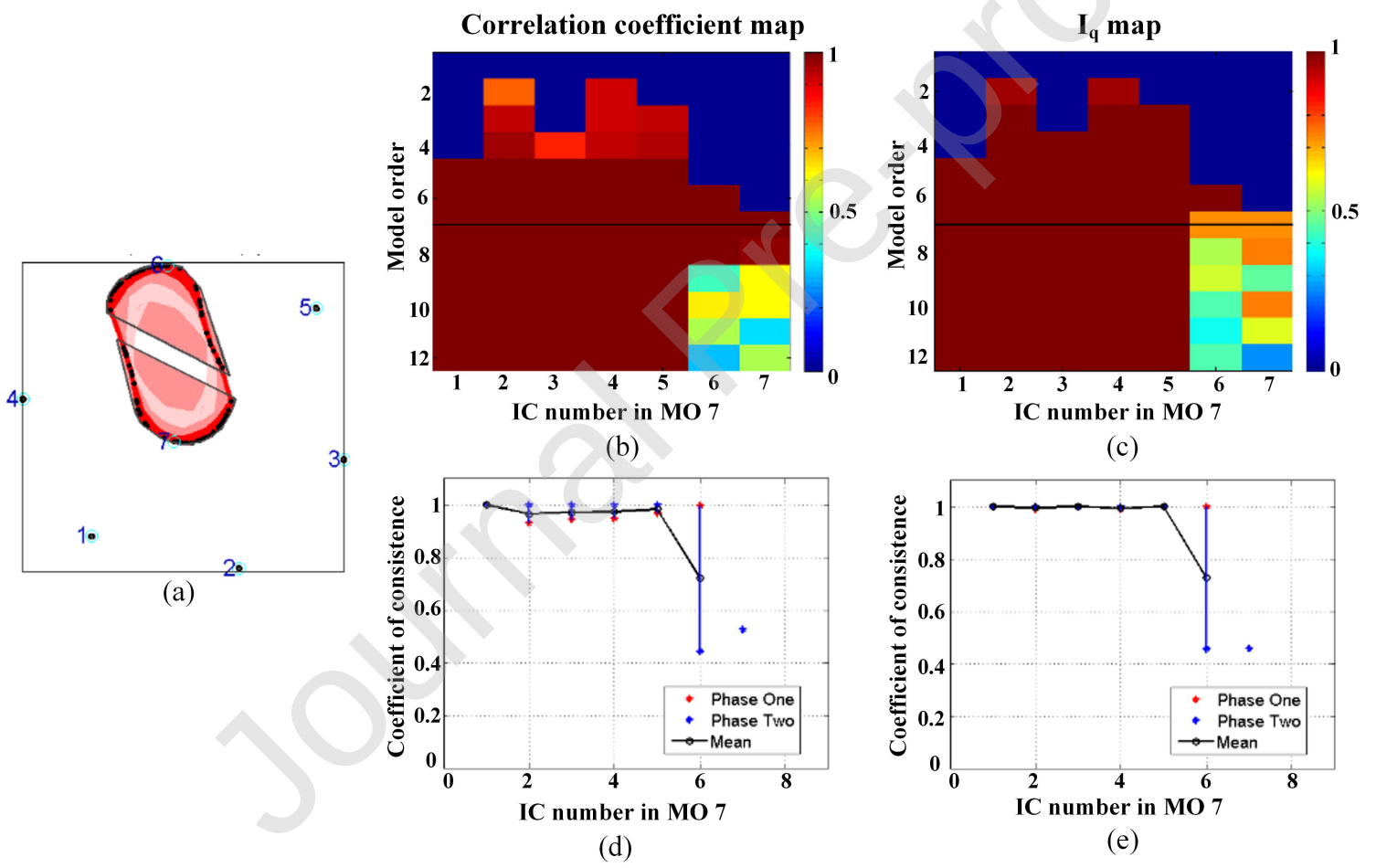

Fig. 3. The results and index figures of FastICA. (a) The tensor clustering result of MO = 7 over 50 runs. Consistent components (in this case 1-5) are compact in this space – the large spatial extent of components 6 and 7 show that their values are not highly consistent. They are projection outcomes from high dimensions, which means the directionality or location are essentially nonsense. (b) Correlation coefficients paired results (c) Rank-1 components index paired results. (d) Consistence index of correlation coefficients. (e) Consistence index of I_q index.

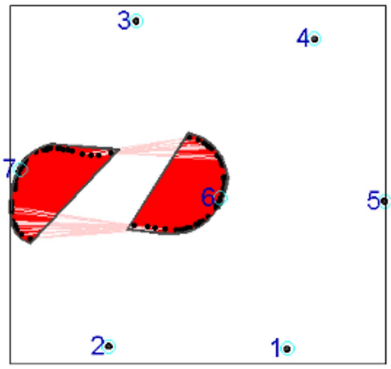

(a)

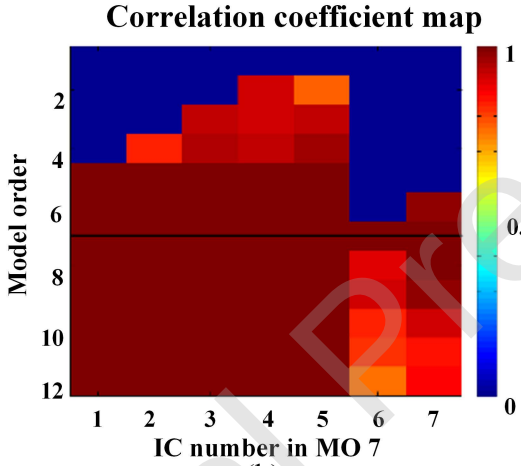

(b)

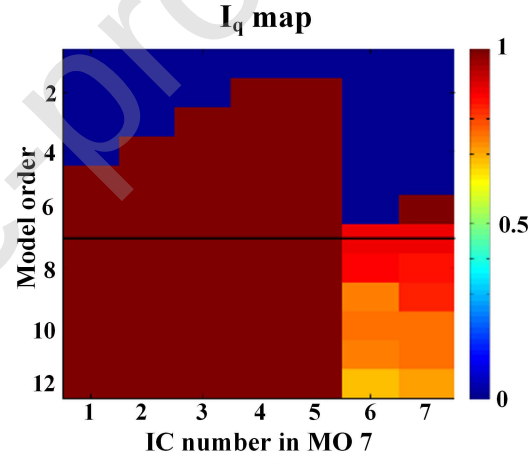

(c)

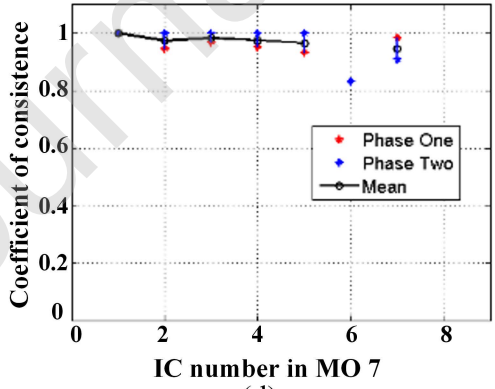

(d)

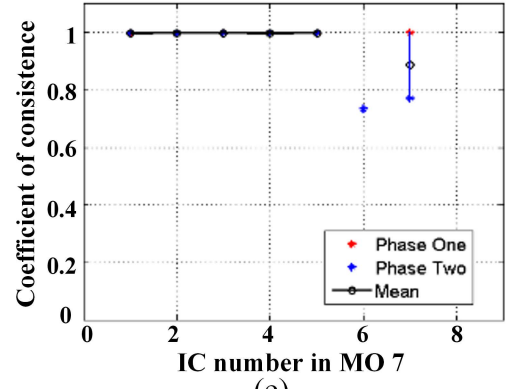

(e)

Fig. 4. The results and index figures of InfomaxICA. (a) The tensor clustering results for MO = 7 over 50 runs. Consistent components (in this case 1-5) are compact in this space – the large spatial extent of components 6 and 7 show that their values are not highly consistent. They are projection outcomes from high dimensions, which means the directionality or location are essentially nonsense. (b) Correlation coefficients paired results (c) Rank-1 components index of paired results. (d) Consistence index of correlation coefficients. (e) Consistence index of I_q index.

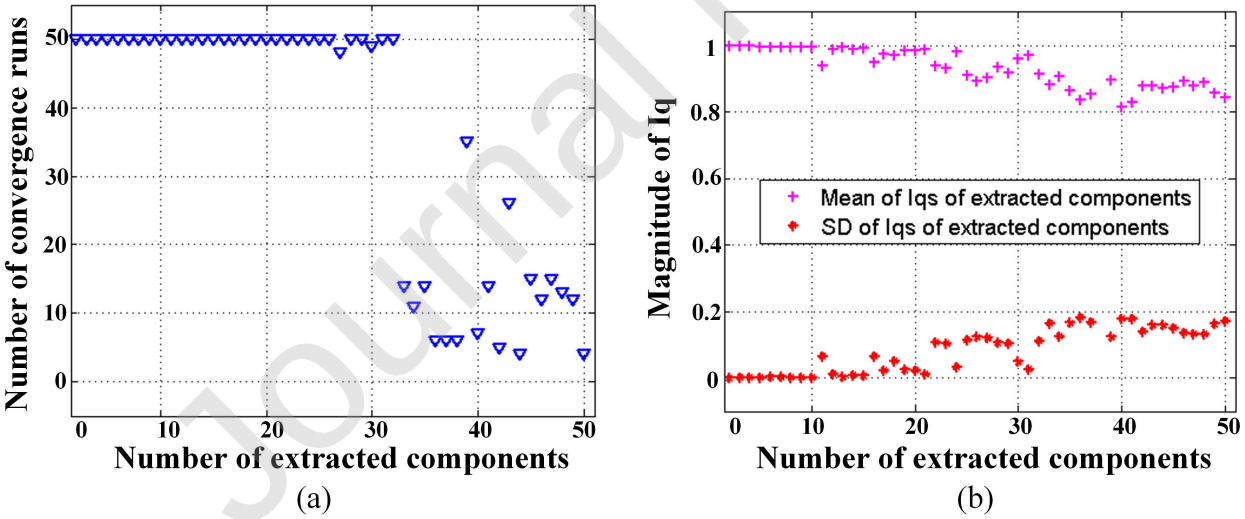

Fig. 5. (a) Number of convergence runs in a total of 50 runs from model order 2-50. The convergence number runs has decreased since model order over 30, indicating the unreliability of decomposition results. (b) The tensor clustering result of the spatial-temporal rank-1 matrix in the same range. The lower of mean Iqs denote a more instable clustering results of ICs under single model order.

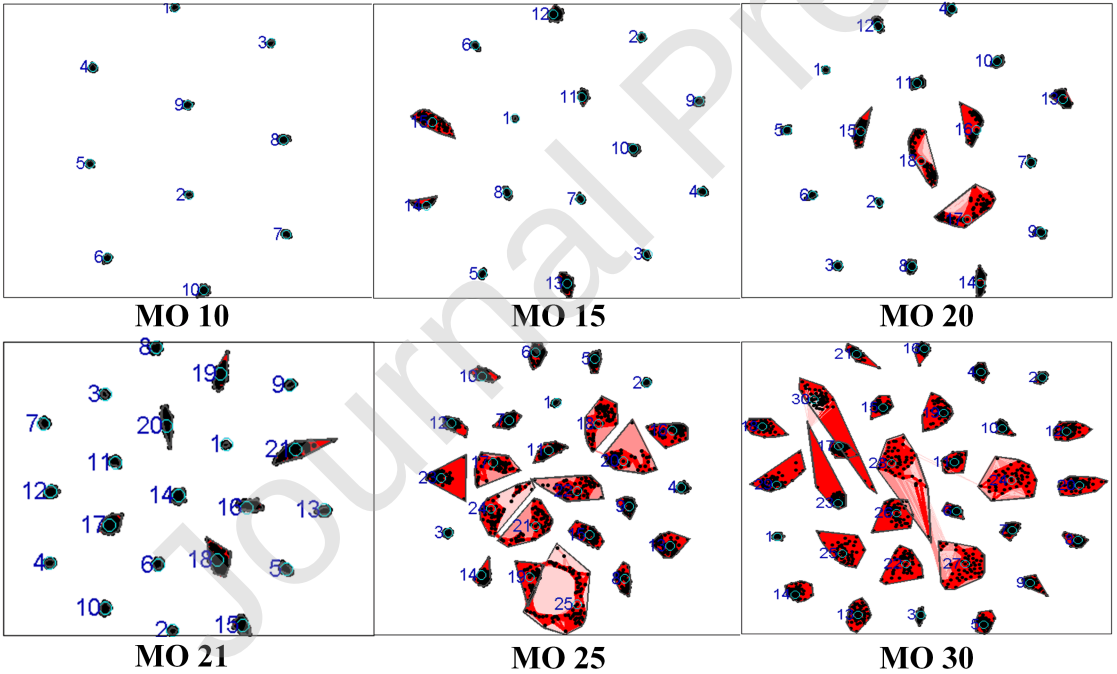

Fig. 6. Visualization for the tensor clustering result in MO 10, MO 15, MO18, MO 21, MO 25 and MO 30. Blue numbers label the extracted ICs, and the black dots (ICs) are clustered within convex hulls. And the centroid is highlighted using blue circle. Red lines connected dots denotes the similarity of them.

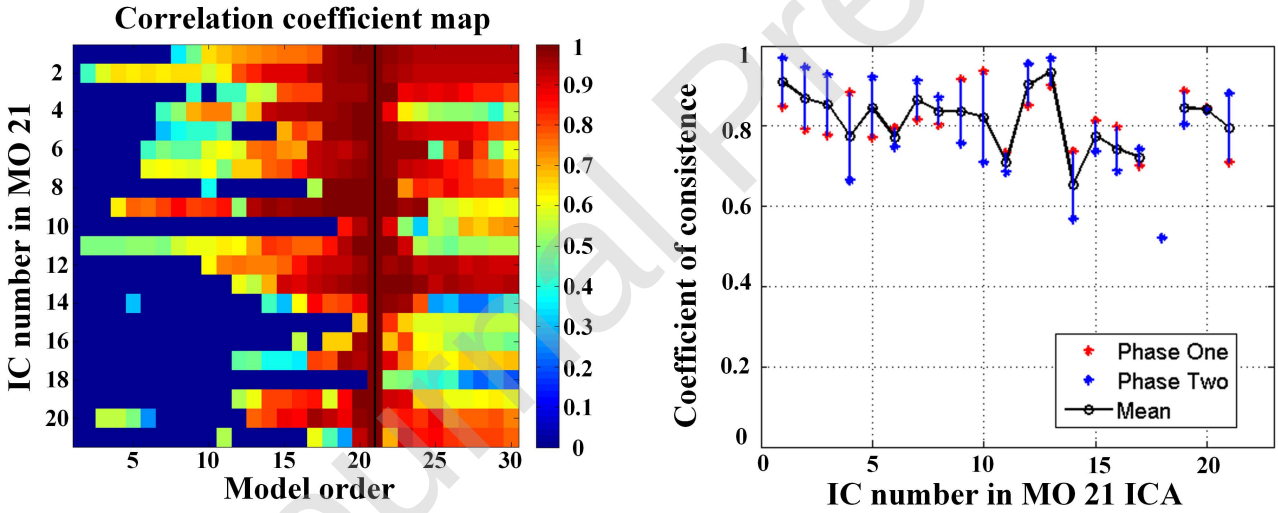

Fig. 7. (a) Paired correlation coefficient results for all IC's found in the optimal MO 21 with components found in model orders over the range from 2-30. Model order increases from left to right. Some components are consistent over all runs – IC#2 and IC#11 appear at MO 2 and persist over all model orders. IC #s 5, 8, 14, 16, 20, and 21 appear in some lower order fits, disappear with increasing model order, and then reappear and persist. Component 18 does not appear until MO 21. The black vertical line shows MO 21 on the y axis – all correlation coefficients are 1 along this line. (b) Consistence quality coefficient in MO 21 address the reliability for each IC. It is clear that there is no Cq for IC#18 in phase one because it's a new IC just appeared since MO 21.

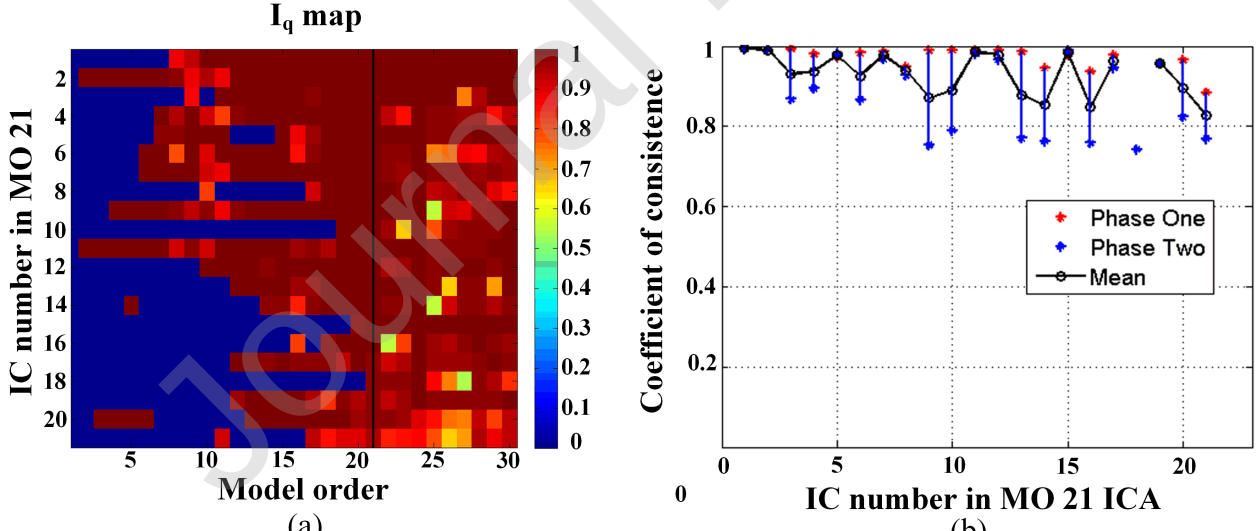

Fig. 8. (a) I_q paired result in optimal MO 21 divided by the black line as the boundary of phase one and phase two. (b) Consistency quality coefficients in MO 21 address the reliability for each IC.

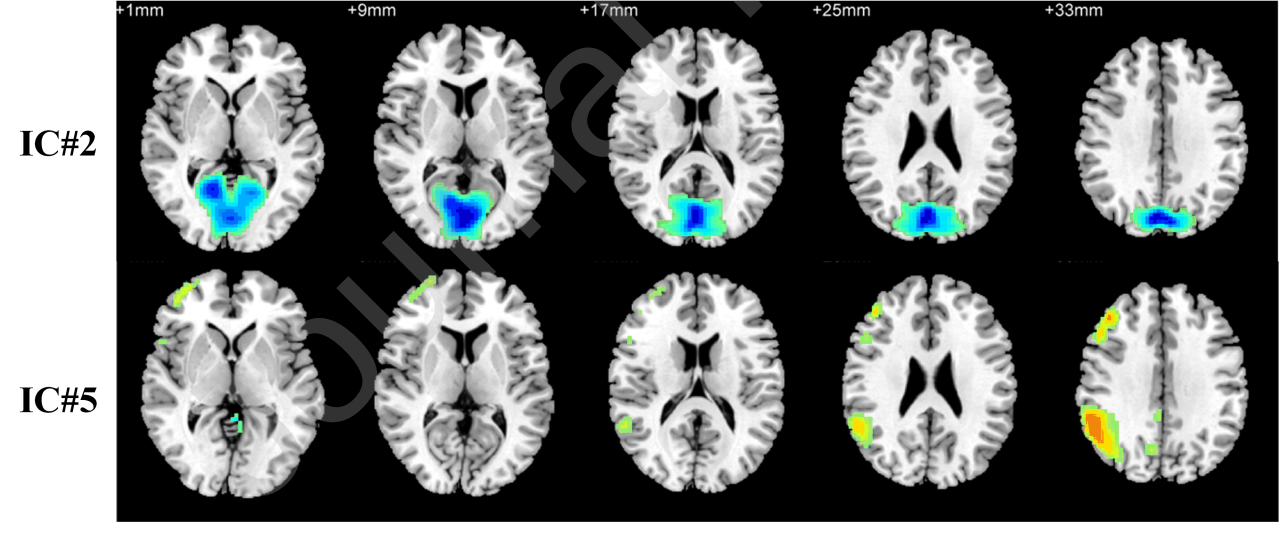

Fig. 9. Spatial maps of IC#2 and IC#5 results (ALFF) in MO#21. Calcarine area in IC#2 and Middle Frontal and Inferior Parietal areas in IC#5.

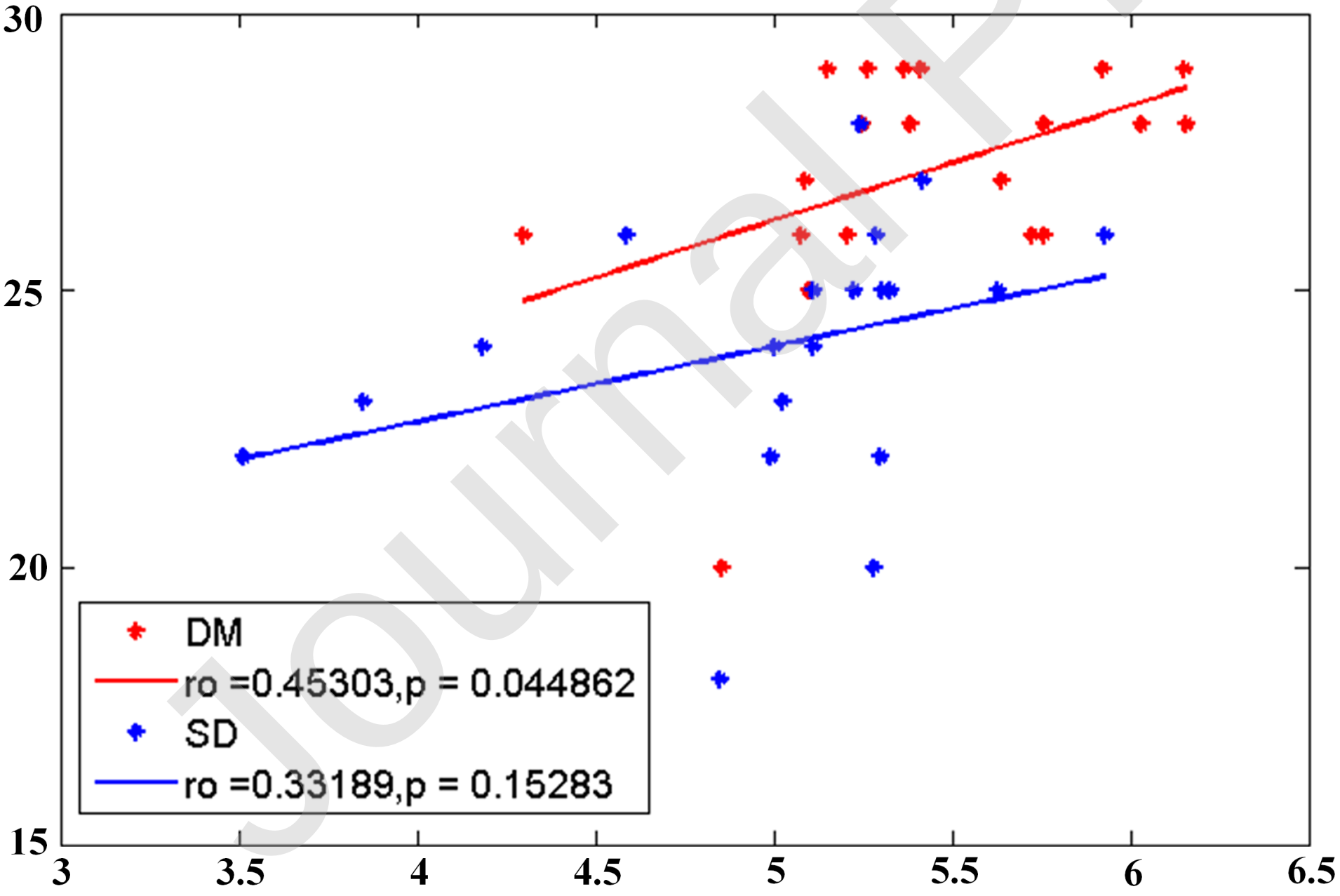

Fig. 10. Tow groups showed positive correlation between MoCA and ALFF of Middle Frontal area in IC#5, and DM is significant with a p-value lower than 0.05.

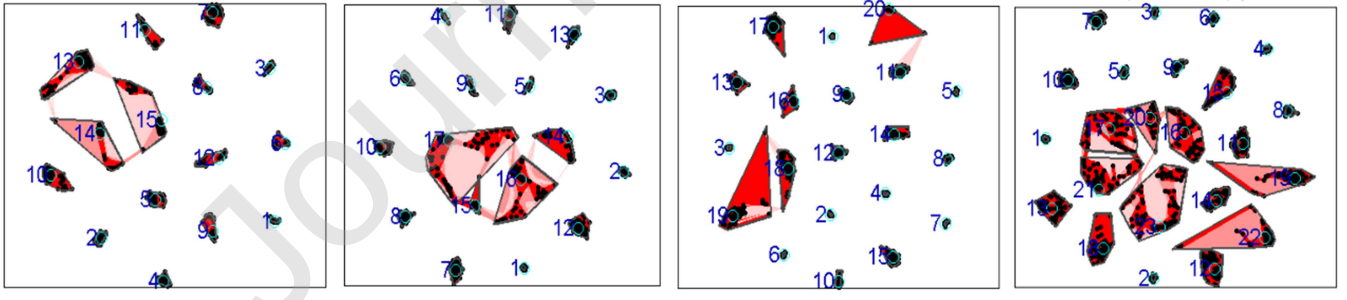

Fig. 11. Visualization for the tensor clustering result in MO 15, MO 17, MO 20, and MO 23. Blue numbers label the extracted ICs, and the black dots (ICs) are clustered within convex hulls. And the centroid is highlighted using blue circle. Red lines connected dots denotes the similarity of them.

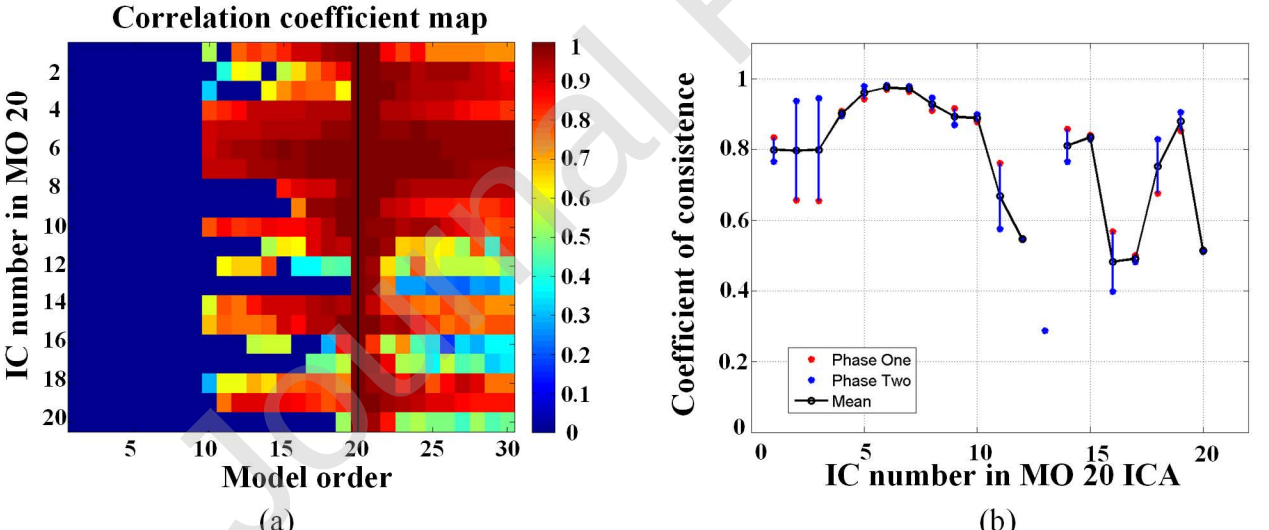

Fig. 12. (a) Paired correlation coefficient results for all IC's found in the optimal MO 20 with components found in model orders over the range from 10-30. Model order increases from left to right. The black vertical line shows MO 20 on the y axis – all correlation coefficients are 1 along this line. (b) Consistence quality coefficient in MO 20 address the reliability for each IC.

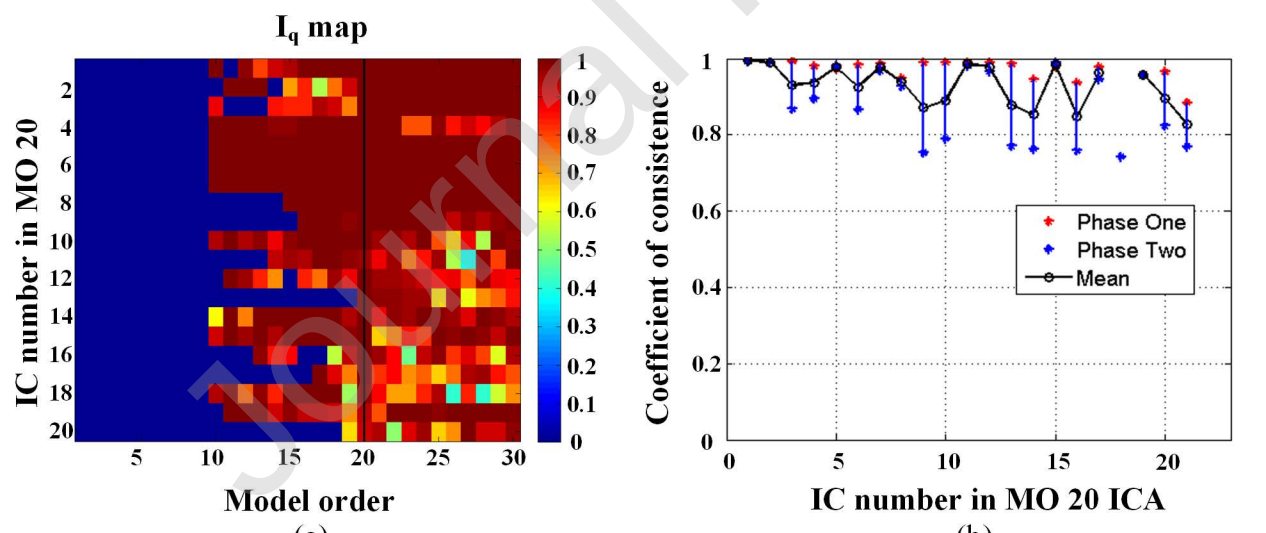

Fig. 13. (a) I_q paired result in optimal MO 20 divided by the black line as the boundary of phase one and phase two. (b) Consistency quality coefficients in MO 20 address the reliability for each IC.

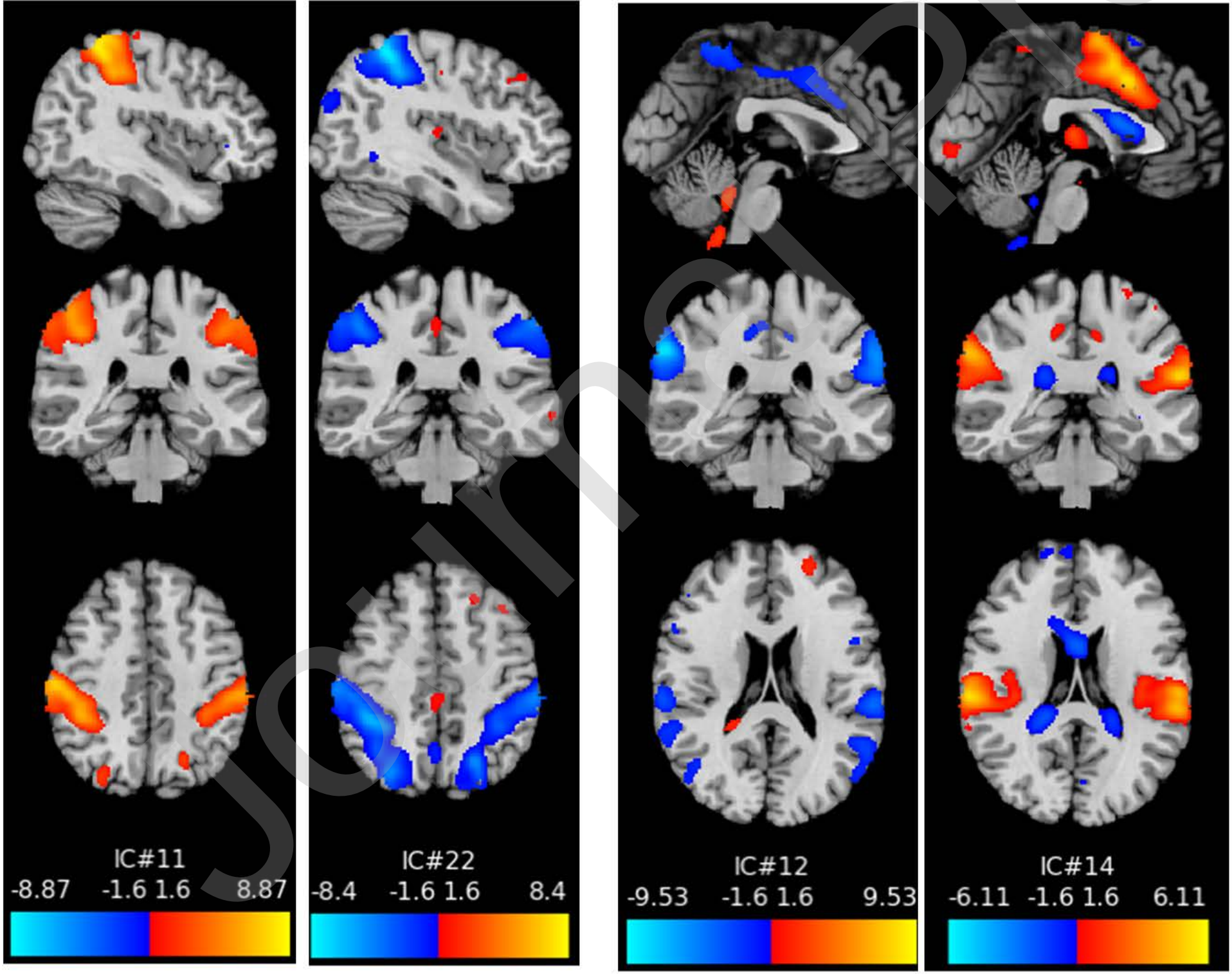

Fig. 14. Spatial maps of IC#11 and IC#12 in MO 20 ICA and their paired components IC#22 and IC#14 in MO 23.The spatial maps were scaled with z-score transformation and thresholded at $|Z|<1.6$.

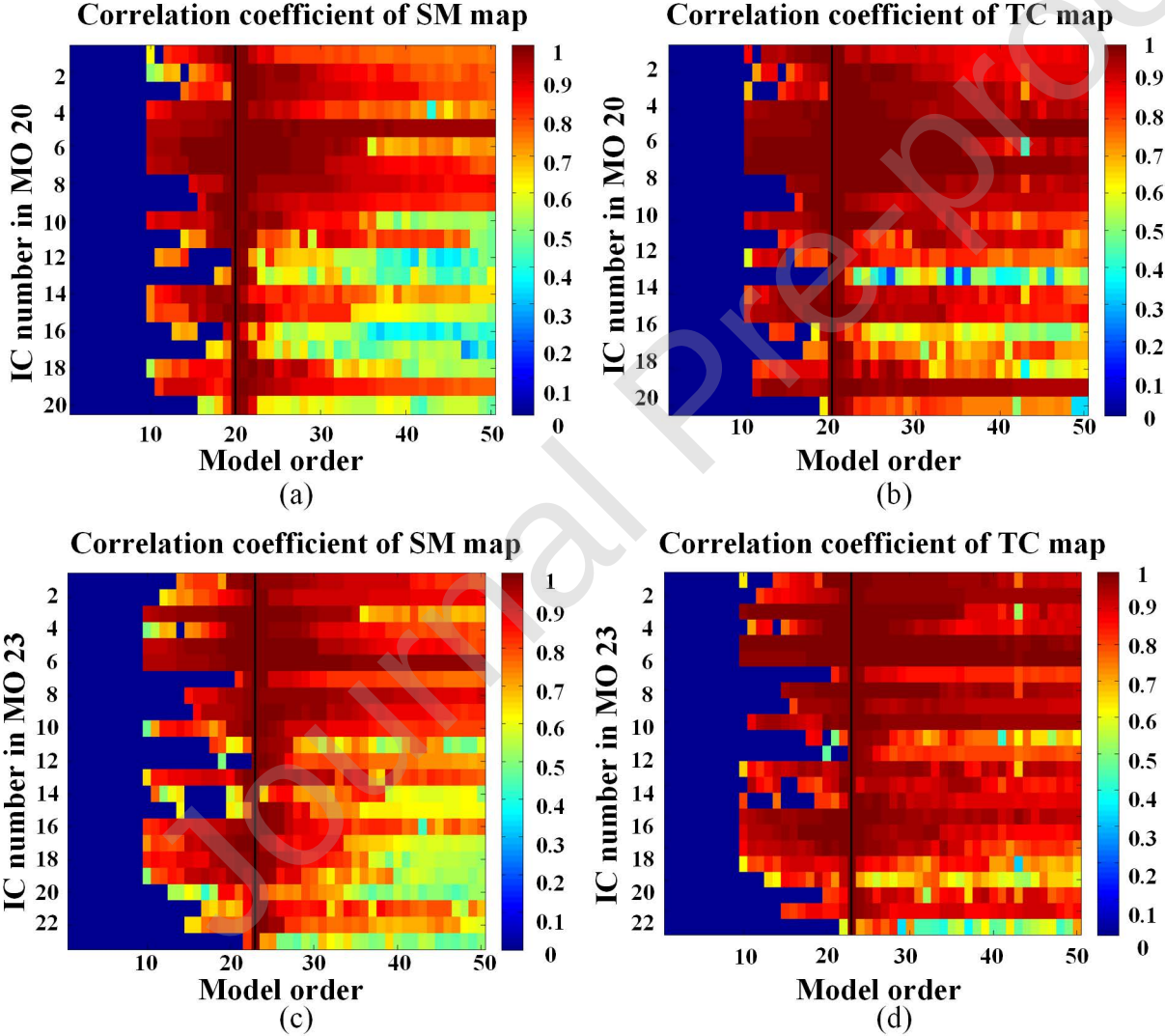

Fig. 15. Paired correlation coefficient results of spatial maps for all IC's found in the optimal MO 20 (a) and in MO 23 (b) with components found in model orders over the range from 10-50. Paired correlation coefficient results of temporal courses for all IC's found in the optimal MO 20 (c) and MO 23 (d) with components found in model orders over the range from 10-50.